

Interpreting the AXP 1E 2259+586 antiglitch as a change in internal magnetization

A. Mastrano^{*}, A. G. Suvorov[†], and A. Melatos[‡]

School of Physics, University of Melbourne, Parkville VIC 3010, Australia

Accepted ?. Received ?; in original form ?

ABSTRACT

The sudden spin-down event (‘anti-glitch’) observed in AXP 1E 2259+586 on 2012 April 21 was arguably caused by a decay of its internal toroidal magnetic field component, which turns a stable prolate configuration into an unstable one. We refine previous models of this process by modelling the star’s magnetic field self-consistently as a ‘twisted torus’ configuration in non-barotropic equilibrium (which allows us to explore a greater range of equilibrium configurations). It is shown that, if the star’s magnetic field is purely dipolar, the change in the toroidal field strength required to produce an anti-glitch of the observed size can be ~ 10 times larger than previously calculated. If the star has a quadrupolar magnetic field component, then an anti-glitch of similar magnitude can be produced via a decay of the quadrupole component, in addition to a decay of the toroidal component. We show that, if the quadrupole component decays, the minimum initial toroidal field strength and the change in toroidal field strength needed to produce the observed anti-glitch are lower than in the pure dipole twisted torus. In addition, we predict the maximum anti-glitch sizes, assuming that they are caused by a change in ellipticity, in four glitching magnetars and discuss the implications for energetics of accompanying X-ray bursts.

Key words: stars: magnetars – stars: magnetic fields – stars: neutron – X-rays: individual: 1E 2259+586

1 INTRODUCTION

All neutron stars undergo electromagnetic braking (Lyne & Graham-Smith 2006). In addition, some neutron stars are observed to undergo sudden, randomly occurring jumps in angular velocity of either sign. Many radio pulsars, as well as five magnetars,¹ exhibit sudden spin ups, known as ‘glitches’ (Espinoza et al. 2011; Yu et al. 2013; Olausen & Kaspi 2014; García & Ranea-Sandoval 2015). One magnetar, the anomalous X-ray pulsar (AXP) 1E 2259+586, has been observed to experience a sudden spin *down*, an ‘anti-glitch’, accompanying an X-ray burst on 2012 April 21 (Archibald et al. 2013). Recently, García & Ranea-Sandoval (2015) proposed that the anti-glitch was caused by a rearrangement of the internal magnetic field of the magnetar: long-term decay of the toroidal field component led to a change from a prolate to another less prolate mass distribution. In this paper, we present a refinement of the García & Ranea-Sandoval model, by constructing a non-barotropic model star in equilibrium, whose density is perturbed by an imposed magnetic field. By considering a non-barotropic model, where pressure is not solely a function of density, we relax some constraints on the magnetic field configuration, allowing a wider range of astrophysical scenarios to be modelled.

Magnetars possess some of the strongest known, naturally occurring magnetic fields (Mereghetti, Pons, & Melatos 2015). The external field strength of a neutron star is usually inferred from its spin down. The internal field, however, cannot be

^{*} E-mail: alpham@unimelb.edu.au

[†] E-mail: suvorova@student.unimelb.edu.au

[‡] E-mail: amelatos@unimelb.edu.au

¹ A list of events is kept at <http://www.physics.mcgill.ca/~pulsar/magnetar/main.html>

measured directly. Observations of bursts and giant flares (Ioka 2001; Corsi & Owen 2011) and precession (Makishima et al. 2014) in magnetars have been interpreted to indicate that the internal field exceeds the external field by at least one order of magnitude. Numerical simulations favour a ‘twisted torus’ magnetic configuration (Braithwaite & Nordlund 2006; Braithwaite & Spruit 2006). Magnetic fields of these strengths deform the stellar mass distribution away from spherical symmetry.

Recently the magnetic deformation of non-barotropic neutron stars has been calculated. Gravitational wave observations (from which we can obtain ellipticity ϵ) can thus be used to infer the internal magnetic structure of neutron stars in principle (Mastrano et al. 2011; Mastrano, Lasky, & Melatos 2013; Mastrano, Suvorov, & Melatos 2015). Because the stars are assumed to be non-barotropic [e.g., due to entropy or lepton fraction gradients (Reisenegger & Goldreich 1992; Reisenegger 2001, 2009)], a greater range of MHD equilibria can be constructed and analysed, and one can easily construct good analytic approximations to the linked poloidal-toroidal twisted torus found in numerical simulations (Braithwaite & Nordlund 2006; Braithwaite 2009; Akgün et al. 2013; Dall’Osso et al. 2015). Although magnetars rotate too slowly to be good gravitational-wave source candidates, the above models can be used to deduce the internal field strengths of fast-rotating newborn magnetars (age $\lesssim 10$ s), which are better candidates for a hypothetical gravitational wave detection from distances as far as the Virgo cluster (Dall’Osso & Stella 2007; Dall’Osso, Shore, & Stella 2009; Mastrano et al. 2011).

The AXP 1E 2259+586 suffered an overall spin frequency change $\approx -5 \times 10^{-7}$ Hz over $\sim 10^2$ d (Archibald et al. 2013). According to Archibald et al. (2013), there are two possible explanations for this event: an anti-glitch with $\Delta\nu/\nu = -3.1(4) \times 10^{-7}$ followed by a glitch with $\Delta\nu/\nu = 2.6(5) \times 10^{-7}$, or an anti-glitch with $\Delta\nu/\nu = -6.3(7) \times 10^{-7}$ followed by another anti-glitch with $\Delta\nu/\nu = -4.8(5) \times 10^{-7}$. Bayesian analysis by Hu et al. (2014) showed that the second explanation, a double anti-glitch, fits the data better. García & Ranea-Sandoval (2015) interpreted the angular velocity drop in terms of a change in ϵ . This interpretation is exciting because it offers a way to infer the internal field strength and structure of AXP 1E 2259+586 independent of other measurements of ϵ , e.g., from future gravitational wave observations of similar objects at the beginning of their lives. However, García & Ranea-Sandoval (2015) used a uniform-density star as the unmagnetized background state, ignored the contribution of the poloidal field component to ϵ , and assumed a uniformly distributed internal field (rather than some self-consistent, spatially varying equilibrium configuration). We relax these restrictions in three ways: we analyse a non-uniform parabolic density distribution [which is sufficient to approximate an $n = 1$ polytropic star: see Mastrano et al. (2011) and Sec. 2.1 of this paper], a non-barotropic hydromagnetic equilibrium, and a linked poloidal-toroidal field structure. We calculate ϵ and explore how much the toroidal field component needs to change to generate the observed anti-glitch magnitude. We also explore the possibility that AXP 1E 2259+586 has a quadrupolar field component, which can contribute to the anti-glitch if it changes.

In Section 2, we recap the non-barotropic deformation calculations in the literature (Mastrano et al. 2011; Mastrano, Suvorov, & Melatos 2015) and apply them to AXP 1E 2259+586 for a dipolar twisted torus configuration. We investigate a range of initial and final states, that give the observed anti-glitch magnitude, comparing our results directly to those of García & Ranea-Sandoval (2015). In Section 3, we construct a dipole-plus-quadrupole twisted torus, apply it to AXP 1E 2259+586, and repeat the test over a range of initial and final states. In Section 4, we calculate the energy released during these changes in field configuration and compare them to the observed outburst energy. We keep the dipole poloidal field strength $B_p = 5.9 \times 10^{13}$ G constant throughout this paper, corresponding to the spin-down-inferred value, as García & Ranea-Sandoval (2015) did. In other words, like they did, we assume that the frequency change is purely due to a decay of the internal toroidal field (Section 2) or the quadrupole component (Section 3), and the dipole poloidal field (which is responsible for overall spin down) remains unchanged before and after the glitch (García & Ranea-Sandoval 2015). In Section 4, we calculate the change in magnetic energy accompanying this process and compare it to the observed X-ray burst energy. In Section 5, we predict the maximum sizes of possible anti-glitches in other magnetars caused by this mechanism and their plausibility. In Section 6, we summarize our results, discuss briefly other possible causes of the anti-glitch, and discuss future work needed to refine the García & Ranea-Sandoval anti-glitch model.

2 DIPOLE TWISTED TORUS

In section 2.1, we summarize the calculation of Mastrano et al. (2011), which relates ϵ to the strength of the toroidal magnetic field component in a non-barotropic star with a twisted torus, whose poloidal component is purely dipolar. In Section 2.2, we apply the results to the AXP 1E 2259+586 anti-glitch.

2.1 Hydromagnetic equilibrium

The magnetic field is assumed to be axisymmetric. It is decomposed into its poloidal and toroidal components and expressed in dimensionless spherical polar coordinates (r, θ, ϕ) as (Chandrasekhar 1956; Mastrano et al. 2011; Mastrano & Melatos 2012; Mastrano, Lasky, & Melatos 2013),

$$\mathbf{B} = B_0[\eta_p \nabla \alpha(r, \theta) \times \nabla \phi + \eta_t \beta(\alpha) \nabla \phi], \quad (1)$$

where B_0 parametrizes the overall strength of the field, η_p and η_t set the relative strengths of the poloidal and toroidal components respectively ($\eta_p = 1$ without loss of generality), $\alpha(r, \theta)$ is the poloidal magnetic stream function, and the function $\beta(\alpha)$ sets the toroidal field component. We consider separable stream functions of the form $\alpha(r, \theta) = f(r)g(\theta)$ in this paper; for a dipolar configuration, one has $\alpha = f(r) \sin^2 \theta$. The radial part of the stream function, $f(r)$, is formally arbitrary, as long as it results in a field that is axisymmetric, continuous everywhere inside the star ($r < 1$), continuous with a current-free dipolar external field at the surface ($r = 1$), finite everywhere, and whose current vanishes at $r = 1$. For analytic simplicity, we choose the polynomial (Mastrano et al. 2011)

$$f(r) = \frac{35}{8} \left(r^2 - \frac{6r^4}{5} + \frac{3r^6}{7} \right). \quad (2)$$

The function β must be a function of α to ensure that the magnetic force has no azimuthal component, which cannot be balanced in magnetohydrostatic equilibrium given a field of the form (1) (Mastrano et al. 2011; Mastrano, Lasky, & Melatos 2013). To conform to the numerical simulations of Braithwaite & Nordlund (2006) and Braithwaite (2009), we want the toroidal component to be confined to a circumstellar torus near the neutral curve, i.e., the circle where the poloidal field component vanishes, located at some radius $r = r_N$ and $\theta = \pi/2$ (with $r_N = 0.79$ for the dipole twisted torus in Sections 2.1 and 2.2). Hence, in keeping with previous works, we choose

$$\beta(\alpha) = \begin{cases} (\alpha - 1)^2 & \text{for } \alpha \geq 1, \\ 0 & \text{for } \alpha < 1. \end{cases} \quad (3)$$

We treat the magnetic force as a perturbation on a background hydrostatic equilibrium and write the hydromagnetic force balance equation as

$$\frac{1}{\mu_0} (\nabla \times \mathbf{B}) \times \mathbf{B} = \nabla \delta p + \delta \rho \nabla \Phi, \quad (4)$$

to first order in $B^2/(\mu_0 p)$, in the Cowling approximation ($\delta \Phi = 0$), where p is the zeroth-order pressure, ρ is the zeroth-order density, Φ is the gravitational potential, and δp , $\delta \rho$, $\delta \Phi$ are perturbations of the latter three quantities. Yoshida (2013) calculated ϵ for a pure dipole without taking the Cowling approximation. His values of $|\epsilon|$ are at most ~ 2 times those found by Mastrano et al. (2011) (depending on the choice of zeroth-order density profile). A thorough, full-perturbation calculation without the Cowling approximation is beyond the scope of this paper.

We do not assume a barotropic star, nor do we solve the Grad-Shafranov equation, so $\delta \rho$ does not have to be a function solely of δp , and therefore the equation of state imposes no restrictions on the field structure. Neutron star matter consists of multiple species which reach a stably stratified, hydromagnetic equilibrium within a few Alfvén time-scales (Pethick 1992; Reisenegger & Goldreich 1992; Reisenegger 2001). This system is not in full chemical equilibrium, however; the relative abundances of the constituent particles change by weak nuclear interactions [time-scale $\sim 10^5 (T/10^8 \text{ K})^{-6} \text{ yr}$] and diffusive processes [time-scale $\sim 10^9 (B/10^{11} \text{ T})^{-2} (T/10^8 \text{ K})^{-6} \text{ yr}$]. Between the Alfvén and the weak nuclear time-scales (Hoyos, Reisenegger, & Valdivia 2008), the star is in a hydromagnetic equilibrium state, in which the composition is not determined solely by the density or pressure, and density and pressure do not correspond one-to-one (Mastrano et al. 2011). Since most magnetars are 1–10 kyr old (as inferred from spin and spin down), the non-barotropic assumption is valid.²

For the zeroth-order density, we choose a parabolic density profile

$$\rho(r) = \rho_c (1 - r^2), \quad (5)$$

where $\rho_c = 15M_*/(8\pi R_*^3)$ is the density at origin, M_* is the stellar mass, and R_* is the stellar radius. This choice is merely for computational simplicity, but, as shown by Mastrano et al. (2011), the resulting ϵ agrees within 5 per cent with that from a more realistic $n = 1$ polytrope.

The stellar ellipticity is given by

$$\epsilon = \frac{I_{zz} - I_{xx}}{I_0}, \quad (6)$$

² Due to the strong inverse dependence of the diffusion and weak nuclear time-scales on temperature, and the rapid cooling of neutron stars over $\sim 10^2$ kyr, chemical equilibrium may never be reached in practice (Yakovlev, Levenfish, & Shibano 1999; Petrovich & Reisenegger 2010, 2011; González-Jiménez, Petrovich, & Reisenegger 2015), so our non-barotropic assumption may be valid for more than just the relatively young magnetars.

where I_0 is the moment of inertia of the unperturbed spherical star, the moment-of-inertia tensor is given by

$$I_{jk} = R_*^5 \int_V d^3x [\rho(r) + \delta\rho(r, \theta)] (r^2 \delta_{jk} - x_j x_k), \quad (7)$$

and the integral is taken over the volume of the star ($r \leq 1$). The density perturbation $\delta\rho$ is calculated by taking the curl of both sides of equation (4) and matching the ϕ -components:

$$\frac{\partial \delta\rho}{\partial \theta} = -\frac{r}{\mu_0 R_*} \frac{dr}{d\Phi} \{ \nabla \times [(\nabla \times \mathbf{B}) \times \mathbf{B}] \}_\phi. \quad (8)$$

For a dipolar twisted torus with $\alpha(r, \theta) = f(r) \sin^2 \theta$, Mastrano et al. (2011) and Mastrano & Melatos (2012) derived the following formula relating ϵ to overall field strength, stellar mass, stellar radius, and the relative poloidal and toroidal field strengths:

$$\epsilon = 5.63 \times 10^{-6} \left(\frac{B_p}{10^{15} \text{ G}} \right)^2 \left(\frac{R_*}{10^4 \text{ m}} \right)^4 \left(\frac{M_*}{1.4 M_\odot} \right)^{-2} \left(1 - \frac{0.351}{\Lambda} \right). \quad (9)$$

In equation (9), B_p is the surface field strength at the pole (for a pure dipole, one has $B_p = 2B_0$), Λ is the ratio of internal poloidal field energy to total internal field energy, $\Lambda = 0$ gives a purely toroidal configuration and $\Lambda = 1$ gives a purely poloidal configuration.

2.2 AXP 1E 2259+586 anti-glitch

Armed with equation (9), we repeat the calculation of García & Ranea-Sandoval (2015), who calculated the change in ϵ as a function of the anti-glitch's frequency change. Section 2 of the latter reference contains the result

$$\frac{\Delta\nu}{\nu} \approx \frac{2}{3} (\epsilon_i - \epsilon_f), \quad (10)$$

where ν is the star's rotation frequency, $\Delta\nu$ is the change in frequency during the anti-glitch, and ϵ_i (ϵ_f) is the initial (final) ellipticity. Equation (10) is derived by assuming that the star initially contains a mostly toroidal field (which induces ϵ_i), which slowly decays by Ohmic diffusion and Hall drift (Viganò et al. 2013). Some critical strain is then reached, when the crust cracks in a sudden event (i.e., the outburst), and the star settles into a new field configuration with $\epsilon_f > \epsilon_i$. The change in frequency (i.e., the anti-glitch) arises from a change in moment of inertia (because angular momentum is conserved), which is then related to the change in ϵ to give equation (4) in García & Ranea-Sandoval (2015), reproduced here as equation (10).

The measured frequency change associated with the anti-glitch is -5×10^{-7} Hz over $\sim 10^2$ d (Archibald et al. 2013). To explain this, Archibald et al. (2013) proposed that the event consisted of (1) an anti-glitch with $\Delta\nu/\nu = -3.1(4) \times 10^{-7}$ followed by a glitch with $\Delta\nu/\nu = 2.6(5) \times 10^{-7}$, or (2) an anti-glitch with $\Delta\nu/\nu = -6.3(7) \times 10^{-7}$ and another anti-glitch with $\Delta\nu/\nu = -4.8(5) \times 10^{-7}$. The second explanation, a double anti-glitch, is statistically favoured (Hu et al. 2014). We take the measured value $\Delta\nu/\nu = -6.3 \times 10^{-7}$ [both for definiteness and to facilitate direct comparison with the results presented in Section 3 of García & Ranea-Sandoval (2015); the calculations can easily be repeated for $\Delta\nu/\nu = -4.8 \times 10^{-7}$] and solve for ϵ_f in equation (10) for various ϵ_i . We present the results in Figs. 1 and 2, to be compared directly to Figs. 1 and 2 of García & Ranea-Sandoval (2015). To facilitate comparison with García & Ranea-Sandoval (2015), we express the toroidal field strength as $\langle B_t \rangle$, i.e., B_t averaged over the volume of the torus. We hold $B_p = 5.3 \times 10^{13}$ G constant, corresponding to the value inferred from spin down, and allow B_t to change.

Figure 1 shows that the toroidal field strength must decrease from its initial value to give an anti-glitch of the observed magnitude, as noted by García & Ranea-Sandoval (2015), with each curve approaching a particular value of $\langle B_t^i \rangle$ as $\langle B_t^f \rangle \rightarrow 0$. This minimum allowed value for $\langle B_t^i \rangle$ is found by setting $\epsilon_f = \epsilon_{\max}$ in equation (10), where the maximum ellipticity ϵ_{\max} is obtained by setting $\Lambda = 1$ (a purely poloidal configuration) in equation (9). However, we require higher initial $\langle B_t^i \rangle$, as well as larger changes in $\langle B_t \rangle$, than predicted by García & Ranea-Sandoval (2015). For example, in order for a star with $M_* = 1.4 M_\odot$ and $R_* = 10^4$ m [solid curves in Fig. 1 in this paper and in García & Ranea-Sandoval (2015)] to give $\Delta\nu/\nu = -6.3 \times 10^{-7}$, the toroidal field must decrease from $\langle B_t^i \rangle = 2 \times 10^{15}$ G to $\langle B_t^f \rangle \approx 8.7 \times 10^{14}$ G, whereas García & Ranea-Sandoval (2015) calculated $\langle B_t^f \rangle \approx 1.8 \times 10^{15}$ G. This is because the poloidal field component tends to deform the star into an oblate shape; neglecting it overestimates the prolateness of the star for a given $\langle B_t \rangle$. This overestimate of ϵ means that, to obtain a given $|\epsilon_i - \epsilon_f|$, we need $\langle B_t \rangle$ to change more than predicted by García & Ranea-Sandoval (2015).

The above behaviour is displayed from an alternative viewpoint in Fig. 2. We plot $-\Delta\nu/\nu$ as a function of the toroidal field strength change $\Delta\langle B_t \rangle / \langle B_t^i \rangle$, where $\Delta\langle B_t \rangle = \langle B_t^i \rangle - \langle B_t^f \rangle$, for three different values of $\langle B_t^i \rangle$, with $B_p = 5.9 \times 10^{13}$ G. In the same plot, the horizontal bands indicate $-\Delta\nu/\nu = 6.3(7) \times 10^{-7}$ (upper band, dark grey) and $-\Delta\nu/\nu = 4.8(5) \times 10^{-7}$ (lower band, light grey). Comparing the solid curve in Fig. 2 with the dashed curve in Fig. 2 of García & Ranea-Sandoval

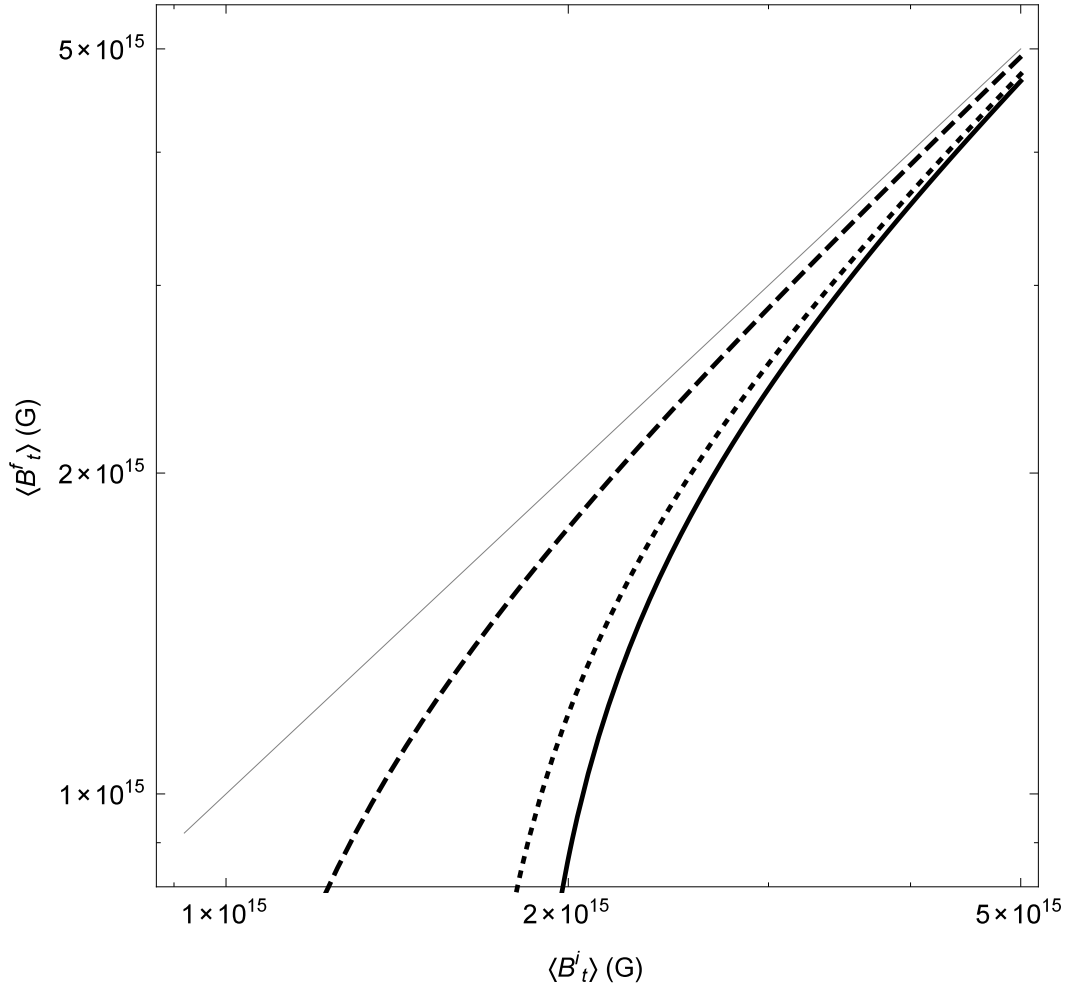


Figure 1. Initial and final toroidal field combinations consistent with the observed anti-glitch in the AXP 1E 2259+586, i.e., solutions to equation (10) for $\Delta\nu/\nu = -6.3 \times 10^{-7}$ [cf. Fig. 1 of García & Ranea-Sandoval (2015)] as a function of initial volume-averaged toroidal field strength $\langle B_t^i \rangle$, for surface polar field strength $B_p = 5.9 \times 10^{13}$ G (inferred from spin down) and three combinations of stellar masses and radii [chosen by García & Ranea-Sandoval (2015)]: $M_* = 1.4M_\odot$, $R_* = 10^4$ m (solid curve); $M_* = 1.4M_\odot$, $R_* = 1.4 \times 10^4$ m (dashed curve); and $M_* = 1.8M_\odot$, $R_* = 1.2 \times 10^4$ m (dotted curve). The thin solid curve is $\langle B_t^i \rangle = \langle B_t^f \rangle$ for reference.

(2015) (both representing $\langle B_t^i \rangle = 2 \times 10^{15}$ G), we see that, to obtain $\Delta\nu/\nu = -6.3 \times 10^{-7}$, our model requires $\Delta\langle B_t \rangle / \langle B_t^i \rangle \approx 50$ per cent, whereas García & Ranea-Sandoval (2015) calculated $\Delta\langle B_t \rangle / \langle B_t^i \rangle \approx 5$ per cent. Thus, by ignoring the poloidal field component, one overestimates $|\epsilon|$ in general and underestimates $\Delta\langle B_t \rangle / \langle B_t^i \rangle$ for a given $|\Delta\nu/\nu|$. For example, for 1.9×10^{15} G $< \langle B_t \rangle < 4.9 \times 10^{15}$ G [corresponding to the minimum value needed for the anti-glitch and the expected limit of stability; see below and Akgün et al. (2013)] and $B_p = 5.9 \times 10^{13}$ G (inferred from spin down), we find $\epsilon/\epsilon_{\text{GRS}} \sim 0.15$, where ϵ is the ellipticity calculated using equation (9) and ϵ_{GRS} is the ellipticity calculated by García & Ranea-Sandoval (2015).

The analytic calculation of Akgün et al. (2013) and the numerical simulation of Braithwaite (2009) found that $10^{-3} \lesssim \Lambda \lesssim 0.8$ is required for a stable dipolar twisted torus. For $B_p = 5.9 \times 10^{13}$ G, this corresponds to 7.7×10^{13} G $\lesssim \langle B_t \rangle \lesssim 4.9 \times 10^{15}$ G. A more stringent limit is set by crust cracking. Horowitz & Kadau (2009) conducted large-scale molecular dynamics simulations of Coulomb solids to represent a neutron star's crust. They found that the large density and pressure make the crust very strong and rigid, capable of supporting $|\epsilon| \lesssim 4 \times 10^{-6}$ (assuming canonical neutron star mass and radius) before cracking suddenly in a collective manner (rather than yielding continuously). If we assume that the initial magnetic field does not deform the star sufficiently to crack the crust, then this limit translates to $\langle B_t^i \rangle \lesssim 3.7 \times 10^{15}$ G in the case of AXP 1E 2259+586. The values of $\langle B_t \rangle$ plotted in Figs. 1 and 2 fall within these relatively generous limits.

3 DIPOLE-PLUS-QUADRUPOLE TWISTED TORUS

Neutron star magnetic fields are approximately dipolar at radio emission altitudes (Lyne & Manchester 1988; Chung & Melatos 2011) and in the outer magnetosphere, where high-energy emissions originate (Romani & Yadigaroglu 1995; Lyutikov, Otte, & McCann

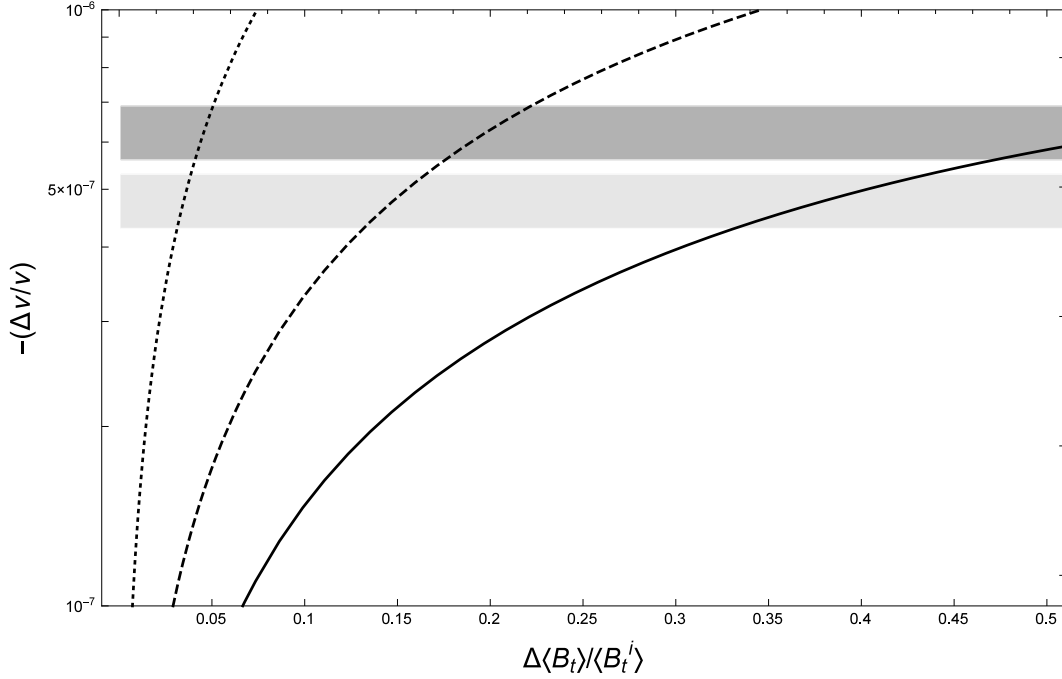


Figure 2. The fractional change in frequency $\Delta\nu/\nu$ as a function of the relative change in the volume-averaged toroidal magnetic field strength $|\Delta\langle B_t \rangle|/\langle B_t^i \rangle$, where $\Delta\langle B_t \rangle = \langle B_t^i \rangle - \langle B_t^f \rangle$ [cf. Fig. 2 of García & Ranea-Sandoval (2015)], i.e., solutions to equation (10) compared to the observed anti-glitch in the AXP 1E 2259+586, for surface polar field strength $B_p = 5.9 \times 10^{13}$ G and three values of $\langle B_t^i \rangle$: 2×10^{15} G (solid curve); 3×10^{15} G (dashed curve); and 4.5×10^{15} G (dotted curve). The bands show $\Delta\nu/\nu$ for the two possible AXP 1E 2259+586 anti-glitch magnitudes inferred from the 2012 April data [taking the statistically favoured double anti-glitch interpretation (Hu et al. 2014)] and their corresponding error bars: $\Delta\nu/\nu = -6.3(7) \times 10^{-7}$ (the initial anti-glitch, dark grey) and $-4.8(5) \times 10^{-7}$ (the follow-up anti-glitch, light grey).

2012). However, some observations can be interpreted as signatures of higher-order multipoles close to the surface (Burnett & Melatos 2014), e.g. cyclotron resonant scattering line energies of certain accretion-powered X-ray pulsars (Nishimura 2005; Priymak, Melatos, & Lasky 2014), radio emissions from pulsars beyond the ‘death line’ (Young, Manchester, & Johnston 1999; Camilo et al. 2000; Medin & Lai 2010), the anomalous braking index of some radio pulsars (Barsukov & Tsygan 2010), and the substructures found in some pulsar signals (Bonazzola, Mottez, & Heyvaerts 2015; Pétri 2015). While the dipole component of the magnetic field can be inferred from the observed spin-down rate, the putative higher-order multipoles contribute small corrections of order $\lesssim (2\pi\nu R_*/c)^2$ to the torque and cannot be measured directly.

In this section, we outline the method used by Mastrano, Suvorov, & Melatos (2015) to describe a self-consistent, linked dipole-plus-quadrupole-plus-toroidal field configuration and to relate the resulting ϵ to $\langle B_t^i \rangle$, $\langle B_t^f \rangle$, and the amplitude of the quadrupolar component.

3.1 Hydromagnetic equilibrium

If the poloidal field is a combination of dipole and quadrupole components, then the stream function $\alpha(r, \theta)$ can be written as a linear combination of the form

$$\alpha(r, \theta) = f_1(r) \sin^2 \theta + \kappa f_2(r) \sin^2 \theta \cos \theta, \quad (11)$$

where κ is a dimensionless parameter controlling the amount of quadrupole field present. In addition to the finiteness and continuity conditions discussed in Section 2.1, $f_1(r)$ and $f_2(r)$ must now be chosen such that the Lorentz force and the resulting density perturbation are continuous everywhere. This is not a trivial task and is best accomplished by moving to a coordinate system defined by the stream function, as described by Mastrano, Suvorov, & Melatos (2015). Suitable $f_{1,2}(r)$ are then found through trial and error. The calculation of ϵ itself is straightforward, using equations (6)–(8). Following Mastrano, Suvorov, & Melatos (2015) for simplicity and consistency, we use

$$f_1(r) = \left(\frac{117}{32} - \sigma \right) r^4 - \left(\frac{65}{16} - 3\sigma \right) r^8 + \left(\frac{45}{32} - 3\sigma \right) r^{12} + \sigma r^{16}, \quad (12)$$

$$f_2(r) = \frac{1}{8} (35r^4 - 42r^8 + 15r^{12}), \quad (13)$$

where σ is a dimensionless free parameter which controls the volume of the torus occupied by the toroidal field component. These $f_{1,2}(r)$ choices are not unique, but they are among the simplest possible polynomials, with the lowest possible order, that guarantee a well-defined field-aligned coordinate transformation.

The stability of dipole-plus-quadrupole configurations has not been calculated, either analytically [like Akgün et al. (2013)] or numerically [like Braithwaite & Nordlund (2006)]. As a consequence, some combinations of σ , κ , and $\langle B_t^{i,f} \rangle$ may be excluded in reality for stability reasons. We defer the numerical calculation (by evolving the field in a time-dependent magnetohydrodynamic simulation) to a future paper.

3.2 AXP 1E 2259+586 anti-glitch

In this section, we repeat the calculation of García & Ranea-Sandoval (2015), except that we assume AXP 1E 2259+586 possesses some quadrupolar magnetic component, which partially decayed during the anti-glitch. In other words, we assume that the change in ϵ which led to the anti-glitch is due to a change in field geometry, in addition to a decay of the toroidal component. We hold $B_0 = 2.95 \times 10^{13}$ G constant, so that the dipolar component's surface polar strength is 5.9×10^{13} G (we thereby assume that the measured spin down, from which a polar field strength of 5.9×10^{13} G is inferred, is due solely to the dipole component). We also set $\sigma = -5$ (for the sake of definiteness), and allow κ and $\langle B_t \rangle$ to change.

In Fig. 3, we show $\langle B_t^f \rangle$ given by equation (10) for $\Delta\nu/\nu = -6.3 \times 10^{-7}$ [cf. Fig. 1 of García & Ranea-Sandoval (2015)] as a function of $\langle B_t^i \rangle$, for $M_* = 1.4M_\odot$, $R_* = 10^4$ m, $B_0 = 2.95 \times 10^{13}$ G, and three different κ_f (final κ) values: $\kappa_f = 0.6$ (solid curve), $\kappa_f = 0.4$ (dashed curve), and $\kappa_f = 0.1$ (dotted curve). We assume $\kappa_i = 0.8$ (initial κ), i.e., that the initial surface quadrupole magnetic field strength at the pole is $1.6B_0$ (surface dipole magnetic field strength at the pole is $2B_0$ as before). This rather extreme value is chosen for the sake of definiteness³. For the dipole-plus-quadrupole twisted torus, ϵ can be written as a function of $\langle B_t \rangle$ according to

$$\epsilon = a \left(\frac{B_0}{10^{13} \text{ G}} \right)^2 \left(\frac{R_*}{10^4 \text{ m}} \right)^4 \left(\frac{M_*}{1.4 M_\odot} \right)^{-2} \left(1 - \frac{b \langle B_t \rangle^2}{B_0^2} \right), \quad (14)$$

where the values of a and b are given as functions of κ in Table 1 (for $\kappa = 0.1, 0.2, 0.4$, and 0.8 ; second and third columns in the table).

Figure 3 tells us that, for a given $\langle B_t^i \rangle$, $\langle B_t^f \rangle$ decreases as κ_f decreases. This is because, in general, the quadrupole component induces more positive (oblate) ϵ : for a given $\langle B_t \rangle$, a configuration with $\kappa = 0.1$ is more prolate (i.e., ϵ more negative) than one with $\kappa = 0.6$, for example. Therefore, a decrease in κ means a decrease in ϵ , which must be countered by a decrease in $\langle B_t \rangle$ (which increases ϵ) to obtain the $(\epsilon_i - \epsilon_f)$ value required to match the observed $\Delta\nu/\nu$ through equation (10). Compared to the pure dipole case of Section 2, however, we find that $\langle B_t^f \rangle$ is generally larger for the mixed case than for the pure dipole case. For example, with $\langle B_t^i \rangle = 2 \times 10^{15}$ G, one finds $\langle B_t^f \rangle = 8.7 \times 10^{14}$ G for the pure dipole case (see solid curve in Fig. 1), but $\langle B_t^f \rangle = 1.8 \times 10^{15}$ G for the $\kappa_i = 0.8$ to $\kappa_f = 0.6$ transition (solid curve in Fig. 3). Note also that, while the general behaviour of the $\langle B_t^i \rangle$ – $\langle B_t^f \rangle$ curves in Fig. 3 are similar to Fig. 1, the minimum values of $\langle B_t^i \rangle$ are smaller for the mixed cases, e.g., $\langle B_t^i \rangle \approx 3 \times 10^{14}$ G for the transitions shown in Fig. 3, compared to 1.8×10^{15} G for the pure dipole case (Fig. 1, solid curve). The decay of the quadrupole plus toroidal components thus provides another channel for the anti-glitch to proceed, one which requires less initial toroidal field strength and less reduction in toroidal field strength, compared to the decay of only the toroidal component in a purely dipolar configuration.

It may be instructive to explore some other possible κ transitions. Because the volume of the torus changes with κ (Mastrano, Suvorov, & Melatos 2015), we find it easier to express our configurations in terms of Λ , the ratio of the poloidal field energy to total field energy. In Fig. 4, we plot some combinations of κ_f and Λ_f (final Λ) which yield $\Delta\nu/\nu = -6.3 \times 10^{-7}$ via equation (10), given initial values $\Lambda_i = 0.1$ and $\kappa_i = 1$ (triangles), 0.8 (pluses), and 0.6 (crosses). There is a clear trend that lower κ_f (for each given κ_i) and higher κ_i (for each given κ_f) need higher Λ_f (i.e., a greater decrease of toroidal component). Figure 4 therefore shows more clearly how the poloidal quadrupole component tends to deform the star into a more oblate shape.

³ Strong higher-order multipoles in magnetars, much stronger than the dipole component (assumed to be the component most responsible for spin down), are not ruled out completely. Analysis of the X-ray spectrum of SGR 0418+5729 suggests that the surface field strength is $\sim 10^2$ stronger than the spin-down-inferred field strength (Rea et al. 2010; Güver, Göğüş, & Özel 2011).

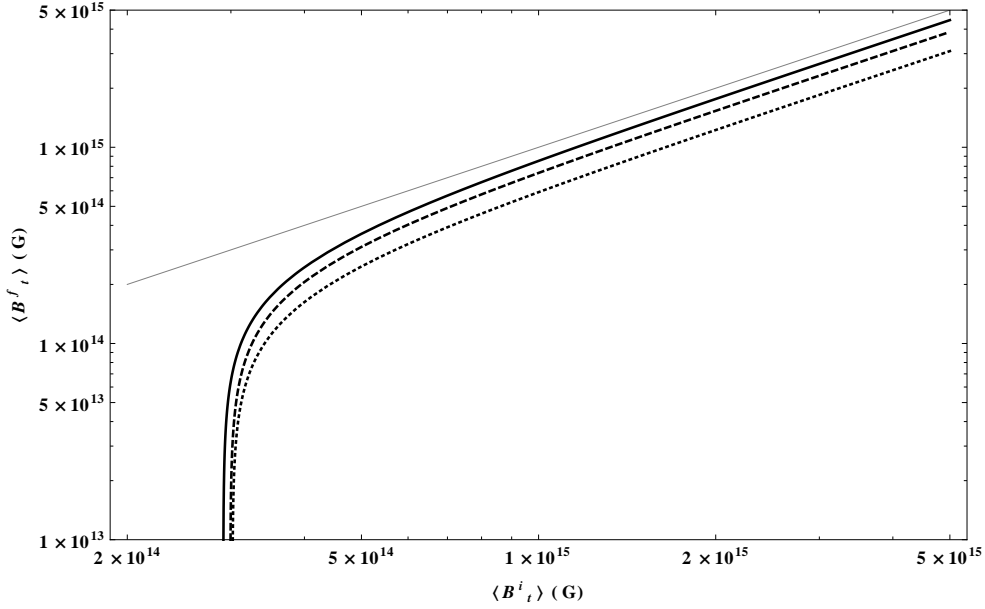


Figure 3. Initial and final toroidal field combinations consistent with the observed anti-glitch in the AXP 1E 2259+586, i.e., solutions to equation (10) for $\Delta\nu/\nu = -6.3 \times 10^{-7}$ [cf. Fig. 1 of García & Ranea-Sandoval (2015)] as a function of initial volume-averaged toroidal field strength $\langle B_t^i \rangle$, for $B_0 = 2.95 \times 10^{13}$ G, $M_* = 1.4M_\odot$, and $R_* = 10^4$ m. The star has a quadrupole component, which decreases in magnitude post-anti-glitch. We keep $\sigma = -5$ and $\kappa_i = 0.8$ (initial κ). The three curves represent different final κ values: $\kappa_f = 0.6$ (solid curve), $\kappa_f = 0.4$ (dashed curve), and $\kappa_f = 0.1$ (dotted curve). The thin solid curve is the identity function, for reference.

Table 1. Values of the parameters a , b , c , and d in the ellipticity and energy formulae, equations (14) and (16). The second and third columns give the values of a and b for different values of κ , given in the first column. The fourth and fifth columns give the values of c and d for transitions from $\kappa = 0.8$ to the values of κ given in the first column.

κ	a (10^{-8})	b	c	d
0.1	9.37×10^{-1}	0.394	4.90	0.63
0.4	9.96×10^{-1}	0.236	4.24	0.73
0.6	1.19	0.149	3.64	0.85
0.8	1.77	0.080	–	–

4 ENERGY

In this section, we calculate the magnetic energy difference between the pre-anti-glitch and post-anti-glitch states and compare it to the observed energy output during the 2012 April 21 burst, which the anti-glitch accompanied (Archibald et al. 2013). For the dipolar case discussed in Section 2, the change in magnetic energy ΔE_m can be written as a function of stellar radius and $\langle B_t \rangle$ as

$$\Delta E_m = 6.59 \times 10^{46} \left(\frac{R_*}{10^4 \text{ m}} \right)^3 \left[\left(\frac{\langle B_t^f \rangle}{10^{15} \text{ G}} \right)^2 - \left(\frac{\langle B_t^i \rangle}{10^{15} \text{ G}} \right)^2 \right] \text{ erg.} \quad (15)$$

For the dipole-plus-quadrupole case described in Section 3, we find

$$\Delta E_m = c \times 10^{46} \left(\frac{R_*}{10^4 \text{ m}} \right)^3 \left[\left(\frac{\langle B_t^f \rangle}{10^{15} \text{ G}} \right)^2 - d \left(\frac{\langle B_t^i \rangle}{10^{15} \text{ G}} \right)^2 \right] \text{ erg,} \quad (16)$$

with the dipole surface polar field strength kept constant at 2.95×10^{13} G. The dimensionless factors c and d are given in Table 1 for three representative transitions from $\kappa_i = 0.8$ to $\kappa_f = 0.1$, 0.4, and 0.6.

During the anti-glitch, the *Fermi* and *Swift* satellites detected an energy release of $E \sim 10^{38}$ erg in the $10\text{--}10^3$ keV band and $E \sim 10^{41}$ erg in the $2\text{--}10$ keV band (Folet et al. 2012; Archibald et al. 2013; Huang & Geng 2014; García & Ranea-Sandoval 2015). We obtain, for both the dipole and dipole-plus-quadrupole configurations, $\Delta E_m \sim 10^{45}\text{--}10^{47}$ erg, similar to the most energetic SGR giant flare (Palmer et al. 2005; Mereghetti 2008). If the anti-glitch was indeed due to a sudden ϵ change, this

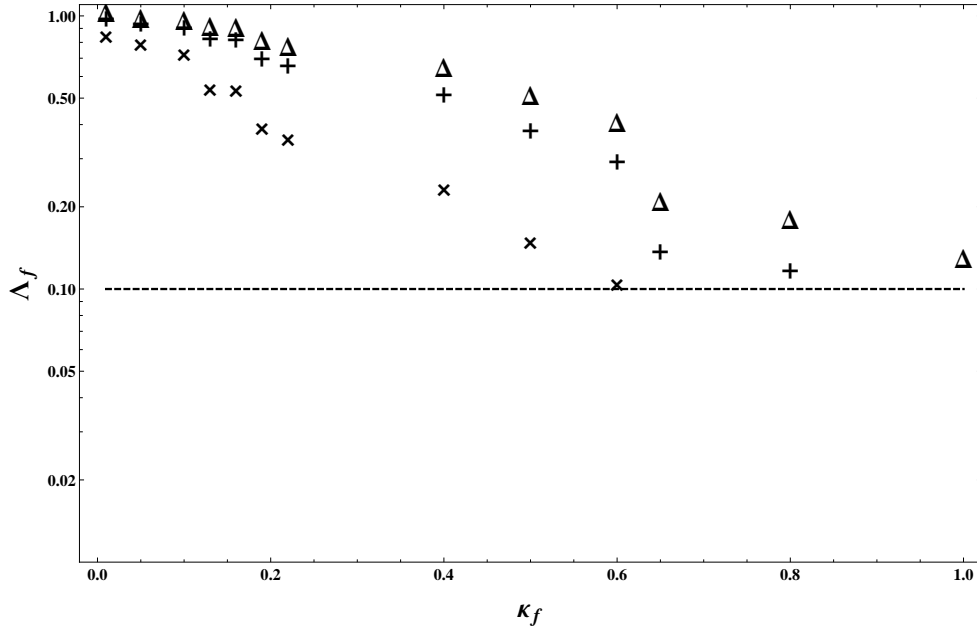


Figure 4. Combinations of κ_f and Λ_f (final values of κ and Λ) which produce the anti-glitch magnitude consistent with that observed in the AXP 1E 2259+586 ($\Delta\nu/\nu = -6.3 \times 10^{-7}$) for a fixed Λ_i (initial Λ). The star is in a dipole-quadrupole twisted torus configuration, with $\Lambda_i = 0.1$ (this initial value of Λ is indicated by the horizontal dashed line, for reference), and $\kappa_i = 1$ (triangles), 0.8 (pluses), and 0.6 (crosses). The dipole surface polar field strength is kept constant at 5.9×10^{13} G (inferred from spin down) and we assume a canonical neutron star mass ($1.4 M_\odot$) and radius (10^4 m).

suggests two possibilities: (1) that, as proposed by García & Ranea-Sandoval (2015), while the crust readjustment process (observed as the anti-glitch) is instantaneous [$\lesssim 1$ d (Archibald et al. 2013)], the magnetic field decay that leads to it is gradual, with time-scale $\sim 10^5$ yr; or (2) that the magnetic energy is released instantaneously, but is inefficiently ($\sim 10^{-5}$) converted into observed electromagnetic energy. As currently there has only been one confirmed anti-glitch, we cannot draw a conclusion yet.

5 ANTI-GLITCHES IN OTHER MAGNETARS?

According to equation (9), we need $B_p \gtrsim 10^{13}$ G to get an anti-glitch of the size observed in AXP 1E 2259+586 with $\Lambda_i = 10^{-3}$ [the lower bound for stability (Akgün et al. 2013)] or with $\epsilon_i = -4 \times 10^{-6}$ [the maximum ellipticity that the crust can tolerate before breaking (Horowitz & Kadau 2009)]. Why, then, have we not observed an anti-glitch from other magnetars, many of which have higher B_p than AXP 1E 2259+586? This is a question that requires a more detailed study and a more sophisticated model than the ones we discuss in this paper. The answer may simply be that we have not yet observed enough objects for long enough, or there may be a more microphysical explanation. Either way, using equations (9) and (10), we can set upper limits on the possible sizes of anti-glitches from other magnetars. Assuming that (1) the magnetic field is in a purely dipolar twisted torus configuration, (2) that the change in ϵ is caused entirely by a change of Λ (or, equivalently, $\langle B_i \rangle$), like in Section 2, (3) that $\epsilon_i = -4 \times 10^{-6}$ (the maximum ϵ that a neutron star’s crust can support before cracking), (4) that $\epsilon_f = \epsilon_{\max}$, and (5) $M_* = 1.4 M_\odot$ and $R_* = 10^4$ m, we write down the maximum possible anti-glitch $(\Delta\nu/\nu)_{\max}$ and the attendant magnetic energy change $(\Delta E_m)_{\max}$ for four magnetars which have exhibited glitches (even though glitches and anti-glitches may be due to entirely different physical processes) and display them in Table 2.

As evident from Table 2, the maximum anti-glitches should be detectable easily by X-ray timing experiments similar to the ones targeting AXP 1E 2259+586. The stronger B_p is, the larger the size of the maximum anti-glitch and the associated magnetic energy change.

The maximum anti-glitches in Table 2 are accompanied by large magnetic energy releases, stronger the one detected during AXP 1E 2259+586 anti-glitch, stronger than the 2004 December 27 giant flare of SGR 1806–20 ($\sim 10^{46}$ erg) (Palmer et al. 2005; Mereghetti 2008). If we assume the magnetic field change is instantaneous and that $\sim 10^{-5}$ of the released magnetic energy is converted into radiation as for AXP 1E 2259+586 (as discussed in Section 4), then we can expect the maximal anti-glitches from these sample magnetars to be accompanied by giant flares with energies $\sim 10^{44}$ – 10^{45} erg. If these putative large anti-glitches are *not* accompanied by energy releases of these magnitudes, we can conclude that, as proposed by

Table 2. Maximum anti-glitch magnitudes $(\Delta\nu/\nu)_{\max}$ and the associated magnetic energy change $(\Delta E_m)_{\max}$ for four glitching magnetars (B_p taken from the McGill magnetar catalog), predicted by assuming that the magnetic field is in a purely dipolar twisted torus configuration, that the change in ϵ is caused entirely by a change of Λ , like in Section 2, and that one has $\epsilon = -4 \times 10^{-6}$ initially [the maximum ellipticity that the crust can support before breaking (Horowitz & Kadau 2009)], that $\epsilon_f = 0$, and $M_* = 1.4 M_\odot$ and $R_* = 10^4$ m.

Name	B_p (10^{14} G)	$(\Delta\nu/\nu)_{\max}$ (10^{-6})	$(\Delta E_m)_{\max}$ (10^{48} erg)
4U 0142+61	1.3	−2.7	-9.2×10^{-1}
1E 1048.1−5937	3.9	−3.0	−1.0
1RXS J170849.0−40091061	4.7	−3.2	−1.1
1E 1841−045	7.0	−3.9	−1.3

García & Ranea-Sandoval (2015), the magnetic fields must decay gradually before the crust cracks and readjusts, or that the electromagnetic conversion efficiency varies substantially across the population.

6 DISCUSSION

In this paper, we refine the model proposed by García & Ranea-Sandoval (2015) to explain the anti-glitch of the AXP 1E 2259+586 in terms of a sudden change in ellipticity ϵ . We also show how the observed anti-glitch can also occur via an alternative magnetic channel, namely the decay of a higher-order multipolar field (in addition to a decay of the toroidal component). We calculate the change in ϵ self-consistently for a dipole twisted torus in Section 2 and a dipole-quadrupole twisted torus in Section 3. We show that, by neglecting the contribution of the poloidal component to the Lorentz force, one overestimates the prolateness of the star (for example, for 1.9×10^{15} G $< \langle B_t \rangle < 4.9 \times 10^{15}$ G and $B_p = 5.9 \times 10^{13}$ G, we find $\epsilon/\epsilon_{\text{GRS}} \sim 0.15$), which leads to an underestimate of the required $\langle B_t^i \rangle$ and the required change in field strength (Figs. 1 and 2). For both dipole and dipole-quadrupole twisted tori, we find that only objects with $B_p \gtrsim 10^{13}$ G (e.g., magnetars) can match the observed $\Delta\nu/\nu$, confirming a conclusion of García & Ranea-Sandoval (2015). This means that we are not likely to observe a similar anti-glitch in a radio pulsar and that, despite superficial similarities, a magnetar anti-glitch may have an entirely different physical origin from a magnetar or pulsar glitch.

If the interior of a neutron star consists of superconducting protons (Lander 2013) or quarks (Glampedakis, Jones, & Samuelsson 2012), then $|\epsilon|$ is raised by a factor of $\sim H_{c1}/\langle B \rangle$, where $H_{c1} \sim 10^{16}$ G is the lower superconductivity critical field (Glampedakis, Andersson, & Samuelsson 2011). In AXP 1E 2259+586, for example, a superconducting interior can raise $|\epsilon|$ by a factor of ~ 10 , lowering the required $\langle B_t^i \rangle$ and $\Delta\langle B_t \rangle$ by a factor of ~ 0.3 . Future anti-glitches, if observed in a star with a lower dipole field inferred from spin down, may be taken as evidence of superconducting interiors.

For ϵ to change by the amount needed to give the observed $\Delta\nu/\nu$ in AXP 1E 2259+586, the magnetic energy change is larger by 5 or 6 orders of magnitude than the observed outburst energy. In Section 5, we calculate the upper limits of anti-glitch magnitudes and energies in four other glitching magnetars (assuming for definiteness that they start at the edge of stability, $\Lambda = 10^{-3}$). We find $(\Delta\nu/\nu)_{\max} \sim 10^{-5}$ – 10^{-3} , higher than the observed AXP 1E 2259+586 anti-glitch, and magnetic energy releases of order 10^{49} – 10^{50} erg, higher than the most energetic magnetar giant flare of $\sim 10^{46}$ erg (Palmer et al. 2005; Mereghetti 2008). If these anti-glitches are observed in the future, we can use the energy of the accompanying burst/flare (if any) to help conclude whether the field reconfiguration is instantaneous but with an inefficient radiative conversion or the field decay is a slow process (García & Ranea-Sandoval 2015). Lander et al. (2015) recently set an upper limit of 4×10^{46} erg on energy released by crustal fracture during a magnetar flare (largely independent of magnetic field strength), assuming the fracture extends to the base of the crust. Therefore, a high-energy flare can, in principle, be powered solely by a ‘crustquake’. Differentiating the energy contributions from crust and field may be difficult in practice, but if a flare is accompanied by an anti-glitch, a significant fraction of the observed energy may be due to field reconfiguration.

The anti-glitch in AXP 1E 2259+586 has also been interpreted as evidence that AXPs and other magnetars are surrounded by fallback matter (Katz 2013). Huang & Geng (2014) proposed that the anti-glitch is due to a collision between AXP 1E 2259+586 and a small solid body with a mass $\sim 10^{18}$ kg. Kantor & Gusakov (2014) suggested instead that the anti-glitch is a consequence of neutron star superfluidity, just like a normal pulsar glitch, due to a velocity lag between the superfluid and the crust. We do not consider these alternative scenarios in this paper.

We also do not model the trigger and time-scale of the anti-glitch. Like García & Ranea-Sandoval (2015), we implicitly assume that the anti-glitch (and the outburst it accompanied) occurred, when the magnetar crust cracked due to some internal instability, built up as the internal toroidal magnetic field decayed (but see also Sections 4 and 5). Link (2014), in contrast, concluded that magnetar bursts and flares must be caused by a relaxation of the *external* field, to be consistent with the rise times of the accompanying quasi-periodic oscillations. Lyutikov (2015) similarly concluded that a magnetar burst/flare can

proceed without any internal instability leading to crust cracking. A simulation of the field decay process, the resultant crust cracking, and a calculation of the time-scales involved are reserved for future work.

ACKNOWLEDGMENTS

We thank the referee for the comments and suggestions, which have improved this manuscript considerably. This work was supported by an Australian Research Council Discovery Project Grant (DP110103347) and an Australian Postgraduate Award.

REFERENCES

- Aasi J. et al., 2015, *Class. Quant. Grav.*, 32, 074001
- Akgün T., Reisenegger A., Mastrano A., and Marchant P., 2013, *MNRAS*, 433, 2445
- Archibald R.F. et al., 2013, *Nat*, 497, 591
- Barsukov D.P. and Tsygan A.I., 2010, *MNRAS*, 409, 1077
- Bonazzola S., Mottez, F., and Heyvaerts J., 2015, *A&A*, 573, A51
- Braithwaite J., 2009, *MNRAS*, 397, 763
- Braithwaite J. and Nordlund Å., 2006, *A&A*, 450, 1077
- Braithwaite J. and Spruit H.C., 2006, *A&A*, 450, 1097
- Burnett C.R. and Melatos A., 2014, *MNRAS*, 440, 2519
- Camilo F., Kaspi V.M., Lyne A.G., Manchester R.N., Bell J.F., D’Amico N., McKay N.P.F., and Crawford F., 2000, *ApJ*, 541, 367
- Chandrasekhar S., 1956, *Proc. Nat. Acad. Sci.*, 42, 1
- Chandrasekhar S. and Fermi E., 1953, *ApJ*, 118, 116
- Chung C.T.Y. and Melatos A., 2011, *MNRAS*, 411, 2471
- Cioffi R., Ferrari V., and Gualtieri L., 2010, *MNRAS*, 406, 2540
- Corsi A. and Owen B., 2011, *PRD*, 83, 104014
- Cutler C., 2002, *Phys. Rev. D*, 66, 084025
- Dall’Osso S. and Stella L., 2007, *Ap&SS*, 308, 119
- Dall’Osso S., Shore S.N., and Stella L., 2009, *MNRAS*, 398, 1869
- Dall’Osso S., Giacomazzo B., Perna R. and Stella L., 2015, *ApJ*, 798, 25
- Espinoza C.M., Lyne A.G., Stappers B.W., and Kramer M., 2011, *MNRAS*, 414, 1679
- Foley S., Kouveliotou C., Kaneko Y., and Collazzi A., 2012, *GRB Coord. Netw.*, 13280, 1
- García F. and Ranea-Sandoval I.F., 2015, *MNRAS*, 449, L73
- González-Jiménez N., Petrovich C., and Reisenegger A., 2015, *MNRAS*, 447, 2073
- Glampedakis K., Andersson N., and Samuelsson L., 2011, *MNRAS*, 410, 805
- Glampedakis K., Jones D.I., and Samuelsson L., 2012, *PRL*, 109, 081103
- Güver T., Göğüş E., and Özel F., 2011, *MNRAS*, 418, 2773
- Haskell B., Samuelsson S., Glampedakis K., and Andersson N., 2008, *MNRAS*, 385, 531
- Horowitz C.J. and Kadau K., 2009, *PRL*, 102, 191102
- Hoyos J., Reisenegger A., and Valdivia J.A., 2008, *A&A*, 487, 789
- Hu Y.-M., Pitkin M., Heng I.S., and Hendry M.A., 2014, *ApJ*, 784, L41
- Huang Y.F. and Geng J.J., 2014, *ApJ Lett*, 782, L20
- Ioka K., 2001, *MNRAS*, 327, 639
- Kantor E.M. and Gusakov M.E., 2014, *ApJ Lett*, 797, L4
- Katz J.I., 2013, *ApSS*, 349, 611
- Lander S.K., 2013, *PRL*, 110, 071101
- Lander S.K., Andersson N., Antonopoulou D., and Watts A.L., 2015, *MNRAS*, 449, 2047
- Link B., 2014, *MNRAS*, 441, 2676
- Lyne A.G. and Graham-Smith F., 2006, *Pulsar Astronomy*. Cambridge University Press, Cambridge
- Lyne A.G. and Manchester R.N., 1988, *MNRAS*, 234, 477
- Lyutikov M., 2015, *MNRAS*, 447, 1407
- Lyutikov M., Otte N., and McCann A., 2012, *ApJ*, 754, 33
- Makishima K., Enoto T., Hiraga J.S., Nakano T., Nakazawa K., Sakurai S., Sasano M., and Murakami H., 2014, *PRL*, 112, 171102
- Mastrano A. and Melatos A., 2012, *MNRAS*, 421, 760
- Mastrano A., Lasky P.D., and Melatos A., 2013, *MNRAS*, 434, 1658

- Mastrano A., Suvorov A.G., and Melatos A., 2015, MNRAS, 447, 3475
Mastrano A., Melatos A., Reisenegger A., and Akgün T., 2011, MNRAS, 417, 2288
Medin Z. and Lai D., 2010, MNRAS, 406, 1379
Mereghetti S., Astron. Astroph. Rev., 2008, 15, 225
Mereghetti S., Pons J.A., and Melatos A., 2015, preprint, arXiv:1503.06313 [astro-ph.HE]
Nishimura O., 2005, PASJ, 57, 769
Olausen S.A. and Kaspi V.M., 2014, ApJS, 212, 6
Palmer D.M. et al., 2005, Nat, 434, 1107
Pethick C.J., 1992, in Pines D., Tamagaki R., Tsuruta S., eds, The Structure and Evolution of Neutron Stars. Addison-Wesley, New York, p. 115
Pétri J., 2015, MNRAS, 450, 714
Petrovich C. and Reisenegger A., 2010, A&A, 521, A77
Petrovich C. and Reisenegger A., 2011, A&A, 528, A66
Priymak M., Melatos A., and Lasky P., 2014, MNRAS, 445, 2710
Rea N. et al., 2010, Sci, 330, 944
Reisenegger A., 2001, ApJ, 550, 860
Reisenegger A., 2009, A&A, 499, 557
Reisenegger A., 2013, preprint, arXiv:1305.2542 [astro-ph.HE]
Reisenegger A. and Goldreich P., 1992, ApJ, 395, 240
Riles K., 2013, PrPNP, 68, 1
Romani R.W. and Yadigaroglu I.-A., 1995, ApJ, 438, 314
Thompson C. and Duncan R.C., 2001, ApJ, 561, 980
Thompson C., Lyutikov M., and Kulkarni S.R., 2002, ApJ, 574, 332
Viganò D., Rea N., Pons J.A., Perna R., Aguilera D.N., and Miralles J.A., 2013, MNRAS, 434, 123
Yakovlev D.G., Levenfish K.P., and Shibano Yu.A., 1999, Phys. Usp., 42, 737
Yoshida S., 2013, MNRAS, 435, 893
Young M.D., Manchester R.N., Johnston S., 1999, Nat, 400, 848
Yu M. et al., 2013, MNRAS, 429, 688

This paper has been typeset from a \LaTeX file prepared by the author.